Articles

Characterization and Activity of Cu-MnO_x/γ-Al_2O_3 Catalyst for Hydrogenation of Carbon Dioxide

QI, Gong-Xin(齐共新) **ZHENG, Xiao-Ming***(郑小明) **FEI, Jin-Hua**(费金华)
HOU, Zhao-Yin(侯昭胤)
Institute of Catalysis, Zhejiang University (Xixi campus), Hangzhou, Zhejiang 310028, China

The effect of manganese on the dispersion, reduction behavior and active states of surface of supported copper oxide catalysts have been investigated by XRD, temperature-programmed reduction and XPS. The activity of methanol synthesis from CO_2/H_2 was also investigated. The catalytic activity over CuO-MnO_x/γ-Al_2O_3 catalyst for CO_2 hydrogenation is higher than that of CuO/γ-Al_2O_3. The adding of manganese is beneficial in enhancing the dispersion of the supported copper oxide and make the TPR peak of the CuO-MnO_x/γ-Al_2O_3 catalyst different from the individual supported copper and manganese oxide catalysts, which indicates that there exists strong interaction between the copper and manganese oxide. For the CuO/γ-Al_2O_3 catalyst there are two reducible copper oxide species; α and β peaks are attributed to the reduction of highly dispersed copper oxide species and bulk CuO species, respectively. For the CuO-MnO_x/γ-Al_2O_3 catalyst, four reduction peaks are observed, α peak is attributed to the dispersed copper oxide species; β peak is ascribed to the bulk CuO; γ peak is attributed to the reduction of high dispersed CuO interacting with manganese; δ peak may be the reduction of the manganese oxide interacting with copper oxide. XPS results show that Cu^+ mostly existed on the working surface of the Cu-Mn/γ-Al_2O_3 catalysts. The activity was promoted by Cu with positive charge which was formed by means of long path exchange function between Cu—O—Mn. These results indicate that there is synergistic interaction between the copper and manganese oxide, which is responsible for the high activity of CO_2 hydrogenation.

Keywords Cu-Mn, CO_2 hydrogenation, XRD, H_2-TPR, XPS.

Introduction

The green house effect of carbon dioxide has been recognized to be one of the serious problems in the world and a number of counter measures have been proposed so far. Catalytic hydrogenation of carbon dioxide into valuable chemical and fuels such as methanol, methane and gasoline has been recently recognized as one of the promising recycling technologies for emitted carbon dioxide. Generally metallic and oxide catalysts have been studied for hydrogenation of carbon dioxide. For example, supported transition metal catalysts such as Ni,[1,2] Rh,[3] Ru[3] are effective for methane formation. Fe[4] and Co[5] catalysts are effective for C^{2+} hydrocarbon formation. Promoted copper catalysts[6-10] are effective for methanol formation (reaction 1).

$$CO_2 + 3H_2 = CH_3OH + H_2O$$
$$\triangle H_{298} = -49.5 \text{ KJ/mol} \quad (1)$$

Methanol is an important basic chemical material produced from mixture of carbon monoxide and hydrogen containing small amounts of carbon dioxide.[11] The growing concern on the green house effect caused by carbon dioxide has motivated laboratory-scale studies of methanol synthesis by the hydrogenation of pure carbon dioxide.[12,13] For methanol synthesis from both carbon monoxide and carbon dioxide, copper-based catalysts, such as Cu-ZnO/Al_2O_3 and Cu-ZnO/Cr_2O_3 have been most widely used. However, under this condition, the utilization of industrial Cu/ZnO/Al_2O_3 catalyst, which exhibited a high activity for methanol synthesis from syn-

* E-mail: cuihua@dial.zju.edu.cn
Received November 30, 2000; revised January 8, 2001; accepted January 15, 2001.
Project supported by Zhejiang Provincial Natural Science Foundation of China.

gas, was not successful.[14] Deng *et al.*[15] reported that the yield of methanol is 7% over the $Cu/ZnO/Al_2O_3$ ultrafine particle catalysts prepared by a novel oxalate gel coprecipitation method under 2.0 MPa, GHSV = 3600 h^{-1}. Few researchers devote themselves to develop a new catalyst or different preparation methods. In the present paper, we reported a study of γ-alumina supported catalysts in an attempt to use these materials for hydrogenation of carbon dioxide to methanol. A system of metallic oxides with copper and manganese was chosen, because these mixed oxides are well known as excellent catalysts in oxidation of carbon monoxide since 1920. The copper/manganese oxide system has mainly been studied as unsupported catalyst. Kotowski, Huang[16-19] reported that CuO/ZnO or Cu/SiO_2 promoted by Mn^{2+} enhanced the turnover of CO. So it is interesting to investigate the activity over the hydrogenation of carbon dioxide. In this paper, the effect of manganese on dispersion, reduction behavior and active state of surface of alumina supported CuO catalysts was investigated by means of the temperature-programmed reduction (TPR), XRD and XPS techniques.

Experimental

Catalyst preparation

The catalysts were prepared by the conventional impregnation method using aqueous solutions of $Cu(NO_3)_2$, $Mn(NO_3)_2$. The support was γ-Al_2O_3, 20-40 mesh. The catalysts were dried at 393 K followed by calcination in an air stream at certain temperature for 4 h. The individual catalyst is denoted as xCu/γ-Al_2O_3 or yMn/γ-Al_2O_3, x, y presented the copper or manganese metal loading in wt%, which is calculated with respect to the weight of γ-Al_2O_3 support.

Measurement of activity for hydrogenation of carbon dioxide

Catalytic activity measurements were carried out by using high pressure micro reactor after introducing pretreatment gas (H_2) at 300℃ for 3 h, the reactant gas was passed through the catalyst bed (2 mL, 20—40 mesh) under a total pressure of 3.0 MPa and a space velocity of 3600 h^{-1}, at certain temperature. The tubing from the catalyst bed to the gas chromatograph was heated at 393 K so as to avoid any condensation of the products. All experimental data were obtained under steady-state conditions that were usually maintained for several hours before changing the reaction temperature to obtain another set of data. The products were analyzed by on-line gas chromatograph with a thermal detector, in which Porapak-Q was used to separate reaction products.

H_2-TPR

TPR measurements were made in a flow system. 10 mg catalyst was pretreated in air at 400℃ and placed in a TPR cell at room temperature, into which H_2-N_2 (5 : 95) mixed gas was introduced. The water produced by the reduction was trapped on a 5A molecular sieve. The temperature of the sample was programmed to rise at a constant rate of 10℃/min and the amount of H_2 uptake during the reduction was measured by a thermal conductivity detector (TCD).

XRD *analysis of crystal phase*

Measurement of X-ray powder diffraction (XRD) was conducted by using a Rigaku D/Max-B for analysis of the crystal phase.

Measurement of photoelectron spectra

Measurement of photoelectron spectra was conducted by using a VG-ESCALAB MKIII surface analyzer, Al K_α, reference to the C(1s) level at 284.6 eV.

Results and discussion

Activity of CO_2 *hydrogenation on* Cu-Mn/γ-Al_2O_3 *catalyst*

Effects of copper loading of Cu/γ-Al_2O_3 *catalysts*

Table 1 shows CO_2 hydrogenation experiment results on Cu/γ-Al_2O_3 catalysts with various copper loading, which was carried out at 3.0 MPa, T = 493 K and GHSV = 3600 h^{-1}, based on the gross catalyst volume.

From Table 1, it can be seen that the activity of Cu/γ-Al_2O_3 catalyst increases with Cu loading from 3 wt% to 12 wt%, then decreases from a higher loading

of Cu. The most active and highest selectivity for methanol is the catalyst with the Cu loading of 12 wt%.

Table 1 Activity of CO_2 hydrogenation on $Cu/\gamma\text{-}Al_2O_3$ catalysts

Catalyst	Conv. of CO_2 (%)	Selectivity (%)			Yield of CH_3OH (%)
		CH_4	CH_3OH	CO	
$3Cu/\gamma\text{-}Al_2O_3$	2.78	2.45	19.57	77.98	0.50
$6Cu/\gamma\text{-}Al_2O_3$	7.03	1.12	19.63	79.26	1.37
$9Cu/\gamma\text{-}Al_2O_3$	7.62	1.0	20.32	78.68	1.54
$12Cu/\gamma\text{-}Al_2O_3$	9.71	0.70	24.03	75.27	2.33
$18Cu/\gamma\text{-}Al_2O_3$	7.80	0.90	23.83	75.27	1.86

Reaction condition: $T = 493$ K, $P = 3.0$ MPa, $H_2/CO_2 = 3/1$, GHSV = 3600 h^{-1}

Effect of manganese loading

Table 2 clearly illustrates the promoting effect of manganese on $Cu/\gamma\text{-}Al_2O_3$ catalyst for the CO_2 hydrogenation. For instance, with the addition of 5 wt% Mn, the conversion of CO_2 and selectivity for CH_3OH increased from 14.6% to 18.7% and from 18.22% to 42.98%, respectively. When the addition of Mn increased to 10 wt%, the catalyst ($12Cu\text{-}10Mn/\gamma\text{-}Al_2O_3$) has the highest activity. This finding attest to Mn's capability to increase the number of active sits for the hydrogenation of CO_2.

Table 2 Effect of manganese loading on activity of CO_2 hydrogenation

Catalyst	Conv. of CO_2 (%)	Selectivity (%)			Yield of CH_3OH (%)
		CH_4	CH_3OH	CO	
$12Cu/\gamma\text{-}Al_2O_3$	14.6	1.50	18.22	80.28	2.66
$12Cu\text{-}5Mn/\gamma\text{-}Al_2O_3$	18.7	1.82	42.98	55.20	8.03
$12Cu\text{-}10Mn/\gamma\text{-}Al_2O_3$	21.9	1.43	45.77	52.80	10.2
$12Cu\text{-}20Mn/\gamma\text{-}Al_2O_3$	19.0	2.0	39.0	59.0	7.4

Reaction condition: $T = 513$ K, $P = 3.0$ MPa, $H_2/CO_2 = 3/1$, GHSV = 3600 h^{-1}

Table 3 shows the particle size of surface Cu, active surface area and dispersion. From Table 3, it can be seen that the dispersion increases with Mn loading from zero to 10%, then decreases slowly. This is because of the addition of Mn which makes the Cu particles smaller and accumulates on the surface, so that the addition of Mn enhances the dispersion of Cu. By comparison of Table 2 and Table 3, it can be seen that the activity of CO_2 hydrogenation is related to the dispersion of CuO. The $12Cu\text{-}10Mn/\gamma\text{-}Al_2O_3$ is the most active catalyst, which has the largest dispersion and the particle size of metallic copper is the smallest.

Table 3 Active area and dispersion of catalysts

Catalysts	Metallic copper particle size (nm)[a]	Active area ($m^2/g.cat$)[17]	Dispersion[17] (%)
$12Cu/\gamma\text{-}Al_2O_3$	52	0.28	0.12
$12Cu\text{-}2.5Mn/\gamma\text{-}Al_2O_3$	9.5	2.72	1.13
$12Cu\text{-}5Mn/\gamma\text{-}Al_2O_3$	6.2	3.56	1.48
$12Cu\text{-}10Mn/\gamma\text{-}Al_2O_3$	5.4	4.10	1.70
$12Cu\text{-}20Mn/\gamma\text{-}Al_2O_3$	5.9	4.00	1.60

[a] Calculate from XRD.

XRD *phase analyses of calcined catalysts*

Fig. 1 shows the XRD profiles of $CuO/\gamma\text{-}Al_2O_3$ catalysts with different Cu contents. From Fig. 1, at low Cu loading (< 6%) no visible CuO crystal phases can be observed; as the CuO loading increasing, the crystal

phase of CuO becomes apparent.

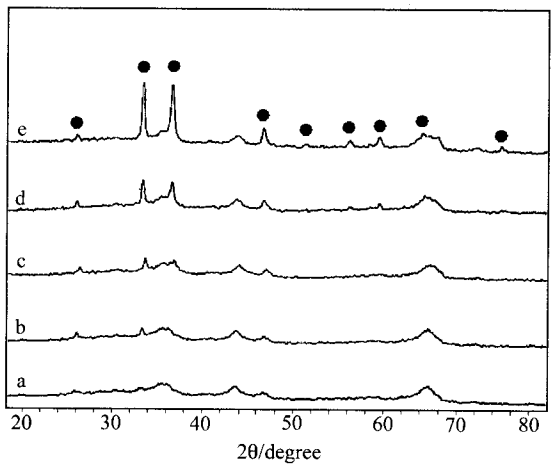

Fig. 1 XRD patterns of $CuO/\gamma\text{-}Al_2O_3$ catalysts with different Cu loading. (a) $3CuO/\gamma\text{-}Al_2O_3$; (b) $6CuO/\gamma\text{-}Al_2O_3$; (c) $9CuO/\gamma\text{-}Al_2O_3$; (d) $12CuO/\gamma\text{-}Al_2O_3$; (e) $18CuO/\gamma\text{-}Al_2O_3$; ● CuO.

Fig. 2 shows the XRD profiles of $MnO_x/\gamma\text{-}Al_2O_3$ catalysts with different Mn content. At low Mn loading (<2.5%) no visible MnO_2 crystal phase can be observed. As the Mn loading increased, the crystal phase of MnO_2 becomes obvious. Fig. 3 shows the XRD profiles of $CuO\text{-}MnO_x/\gamma\text{-}Al_2O_3$ catalysts (12 wt% Cu loading is consistent) with different Mn content. XRD (Fig. 3) results show that the addition of Mn result in a weaker and broader XRD intensity of copper oxide. For supported crystalline oxide, particle size is proportional to its signal intensity of XRD. Hence, doping manganese into $CuO/\gamma\text{-}Al_2O_3$ is beneficial in enhancing the dispersion of the supported copper oxide. The calculated Cu crystallite sizes are listed in Table 3. These values are in coincidence with the results of XRD (Fig. 3). Obviously, there is a decrease in the CuO crystallite size with the addition of manganese oxide. However, it must be emphasized that, while X-ray line broadening measurements are useful as a relative measure of the average crystallite size, the Scherrer formula should not be used for absolute determinations due to its failure in accounting for the effects of microstrain, the consequences of particle size distribution, and the uncertainty in correcting for instrumental broadening. Hence, the values listed in Table 3 are used for comparison only. In a word, the transformation between bulk crystallite CuO and non-crystallite phase took place as the addition of manganese oxide.

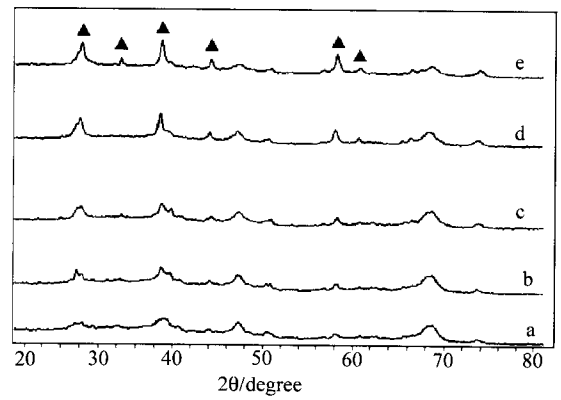

Fig. 2 XRD patterns of $MnO_x/\gamma\text{-}Al_2O_3$ catalysts with different Mn loading. (a) $1.25Mn/\gamma\text{-}Al_2O_3$; (b) $2.5Mn/\gamma\text{-}Al_2O_3$; (c) $5Mn/\gamma\text{-}Al_2O_3$; (d) $10Mn/\gamma\text{-}Al_2O_3$; (e) $20Mn/\gamma\text{-}Al_2O_3$; ▲ MnO_2.

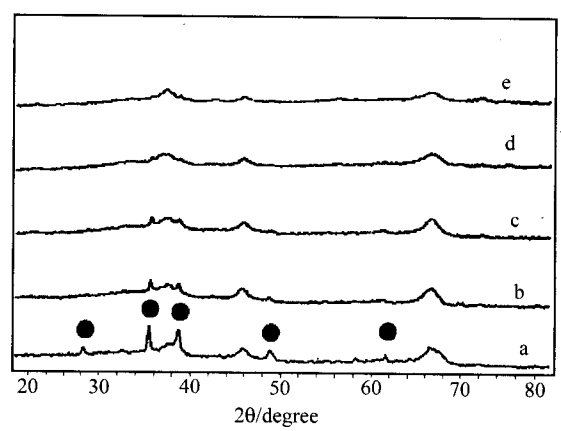

Fig. 3 XRD patterns of $CuO\text{-}MnO_x/\gamma\text{-}Al_2O_3$ catalysts with different Mn loading. (a) $12Cu/\gamma\text{-}Al_2O_3$; (b) $12Cu\text{-}2.5Mn/\gamma\text{-}Al_2O_3$; (c) $12Cu\text{-}5Mn/\gamma\text{-}Al_2O_3$; (d) $12Cu\text{-}10Mn/\gamma\text{-}Al_2O_3$; (e) $12Cu\text{-}20Mn/\gamma\text{-}Al_2O_3$; ● CuO.

XRD analyses of reduced catalysts

When the $CuO/\gamma\text{-}Al_2O_3$, $CuO\text{-}MnOx/\gamma\text{-}Al_2O_3$ catalysts were reduced by H_2 at 300℃, it can be found that XRD (Fig. 4) lines for CuO were absent for the reduced sample while diffraction lines for Cu^0 were present. This indicates that CuO in the catalysts was completely reduced to metallic copper (Cu^0). The mean crystallite sizes were determined by the Scherrer equation, $d = \kappa\lambda/\cos\theta$, and the results are listed in Table 3. This shows that the mean crystallite size of metallic copper in $Cu\text{-}Mn/\gamma\text{-}Al_2O_3$ is much smaller than that in $CuO/\gamma\text{-}Al_2O_3$ and decreases with the increasing manganese content until the ratio of Mn/Cu is 1. The mean particle sizes of metallic copper determined by X-ray

diffraction are consistent with those calculated by specific area of metallic copper (see Table 3). The diffraction line of Cu is broadened, suggesting that Cu atoms were highly dispersed and exhibited "X-ray amorphous" features due to the formation of amorphous or microcrystallite during reduction. Kalier *et al.*[20,21] have also observed the broadening or the absence of X-ray diffraction lines and suggested that Cu was highly dispersed and a considerable amount of amorphous phase was found. It is consistent with our observations.

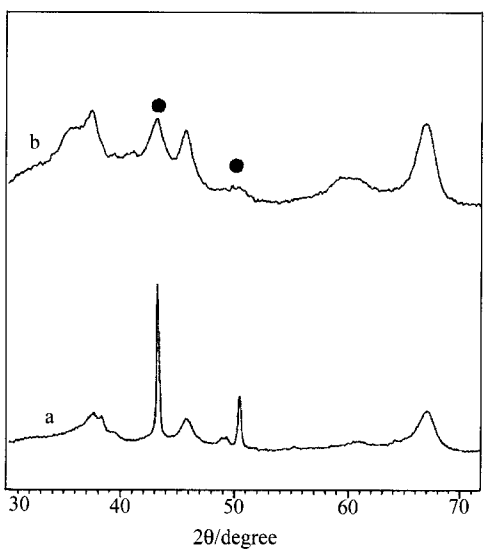

Fig. 4 XRD patterns of reduced 12Cu/γ-Al_2O_3 and 12Cu-10Mn/γ-Al_2O_3. (a) 12Cu/γ-Al_2O_3; (b) 12Cu-10Mn/γ-Al_2O_3.

H_2-TPR *of* CuO/γ-Al_2O_3 *catalysts*

With increasing copper loading, two reduction peaks, namely α and β as shown in Fig. 5, can be observed in the TPR patterns. The area of β peak obviously increases with increasing the copper loading, but the area of α peak has a maximum value occurring at 12 wt% Cu, when the copper loading is lower than 12 wt%, the β-peak area is smaller than that of β-peak, and when the copper loading is higher than 12% the β-peak area is larger than that of α-peak and the α-peak becomes a shoulder. In addition, overlap of α and β peaks becomes very serious when copper loading is higher than 18 wt%. It seems to have a saturated phenomenon occurring at 12 wt% Cu for β-peak. The serious overlap of α and β peaks implies that the reducibility of these two types of copper oxide species gradually approaches to the same.

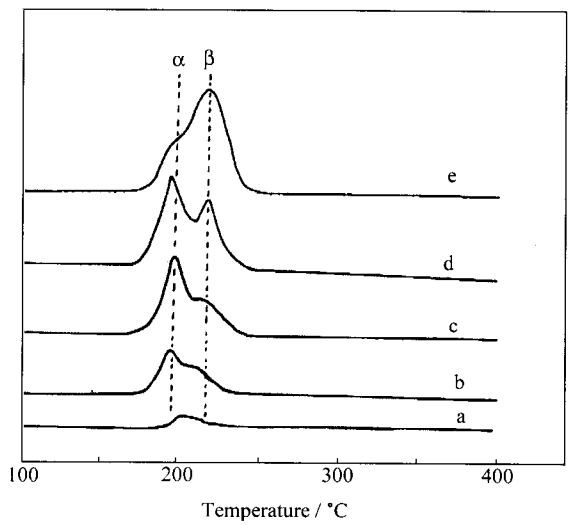

Fig. 5 TPR patterns of CuO/γ-Al_2O_3 catalysts with various Cu loading. (a) 3.0%; (b) 6.0%; (c) 9.0%; (d) 12%; (e) 18%.

Combining the results of TPR and XRD, it can be found that the higher the copper loading is, the larger the β-peak area of TPR and the larger the signal intensity of XRD (Fig. 1). While there is a maximum area of TPR appearing at 12 wt% Cu. These strongly suggest that the α-peak copper oxide species belong to the bulk CuO and the β-peak copper oxide species is contributed to the dispersed CuO.

Friedman *et al.*[22] reported that for CuO/γ-Al_2O_3 catalysts, saturation of the support surface occurs at a copper loading approximately 4—5 wt% Cu per 100 m^2/g Al_2O_3. Above the threshold loading, formation of crystalline CuO is observed. According to Friedman's saturation value, 'monolayer' coverage of supported employed in this study (BET area = 230 m^2/g) should occur at a copper content of approximately 9.2—11.5 wt%. This value is compatible with the TPR results, which have displayed the maximum area of the α peak occurring at 12 wt% Cu, hence, the α and β peak can be unambiguously attributed to the reduction of highly dispersed copper oxide species and bulk-like CuO, respectively.

H_2-TPR *of* CuO-MnO_x/γ-Al_2O_3 *catalyst*

The reduction profile (Fig. 6) of MnO_x/γ-Al_2O_3 is

characterized by two prominent peaks, at 320℃ and 370℃ respectively. The lower temperature peak attributes to the reduction of MnO_2 to Mn_3O_4; the high temperature peak attributes to the reduction of Mn_3O_4 to MnO.[23] For the thermodynamic reasons, further reduction of MnO does not occur under the applied experimental conditions. This result is consistent with the reference.[23]

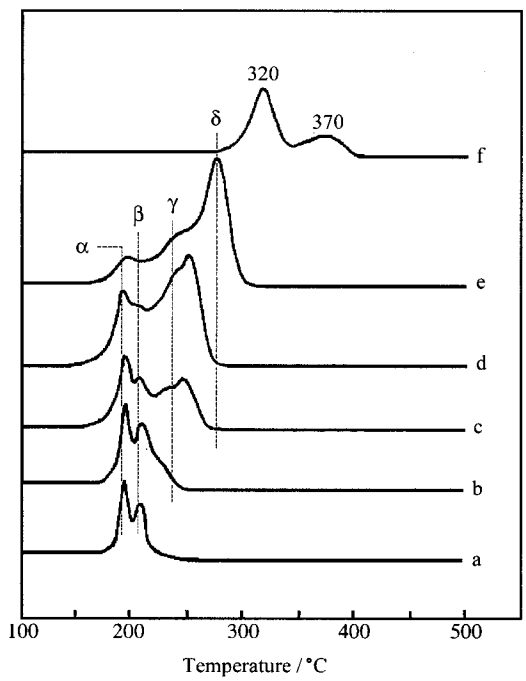

Fig. 6 TPR patterns of $CuO\text{-}MnO_x/\gamma\text{-}Al_2O_3$ with various Mn loading. (a) $12Cu/\gamma\text{-}Al_2O_3$; (b) $12Cu\text{-}2.5Mn/\gamma\text{-}Al_2O_3$; (c) $12Cu\text{-}5Mn/\gamma\text{-}Al_2O_3$; (d) $12Cu\text{-}10Mn/\gamma\text{-}Al_2O_3$; (e) $12Cu\text{-}20Mn/\gamma\text{-}Al_2O_3$; (f) $10Mn/\gamma\text{-}Al_2O_3$.

The TPR profiles of the mixed compounds were also shown in Fig. 6. From the Fig. 6, it can be seen that the reduction position of $CuO\text{-}MnO_x/\gamma\text{-}Al_2O_3$ catalysts lies in between the $CuO/\gamma\text{-}Al_2O_3$ and the $MnO_x/\gamma\text{-}Al_2O_3$. Apparently, manganese retards the reduction of copper as indicated by the shift of the corresponding peak to higher temperatures with increasing manganese content, as the same time, copper enhances the reducibility of manganese because of hydrogenation spillover. The results indicate that there exists an interaction between the copper and manganese oxide, which is consistent with the result of XRD.

From the Fig. 6, it can be seen that when the manganese loading is lower than 2.5%, three peaks are observed and when the manganese loading is higher than 2.5% four peaks are observed. The four peaks are designated by α, β, γ and δ in Fig. 6. The position of α and β peaks remain unchanged with increasing manganese loading. The intensities of α and β peaks decrease rapidly with an increase in manganese loading from 2.5% to 20%. The XRD results (Fig. 1) show that as the addition of manganese increasing, the CuO peaks get lower and lower. Comparison to the TPR results of $CuO/\gamma\text{-}Al_2O_3$ (Fig. 5) we propose that α and β species are contributed to the highly dispersed CuO and larger particle bulk CuO species respectively.

From the Fig. 6, it can be seen that the position of γ peak remains unchanged with increasing manganese loading, while, the intensity of γ peak increases with the increasing manganese loading. We propose that the γ species is ascribed to the high dispersed CuO interacting with Mn oxide. The area of δ peak monotonously increases with increasing manganese loading and shifts to higher temperature. On the basis of XRD results and these findings, it is concluded that the peak δ may be ascribed to the reduction of manganese oxide interacting with copper oxide.

The TPR results show that there exists strong interaction between the copper and manganese oxide which causes the TPR peak of the $CuO\text{-}MnO_x/\gamma\text{-}Al_2O_3$ catalyst different from the individual supported copper and manganese oxide catalysts.

Surface state of activity

The XPS of the Mn(2p) level for the calcined, reduced and used catalysts are shown in Fig. 7. From Fig. 7, it can be seen that the binding energy (B.E.) of the Mn(2p) level for the calcined catalyst was very close to that for pure Mn_2O_3 (B.E. = 642). On the other hand, in the reduced catalyst, the B.E. value of the Mn(2p) band was decreased, which is contributed to the MnO. For the used catalyst, it is found that two peaks appear, one shows a B.E. of 641.5 eV and another a B.E. of 642 eV, the latter peak contributes to MnO_2. Based on the results mentioned above, it is concluded that the valence of Mn is + 2 after reduction, while it increases to + 3 and + 4 after reaction. The XPS of the Cu(2p) level for the calcined, reduced and used catalysts are shown in Fig. 8. From Fig. 8, it can

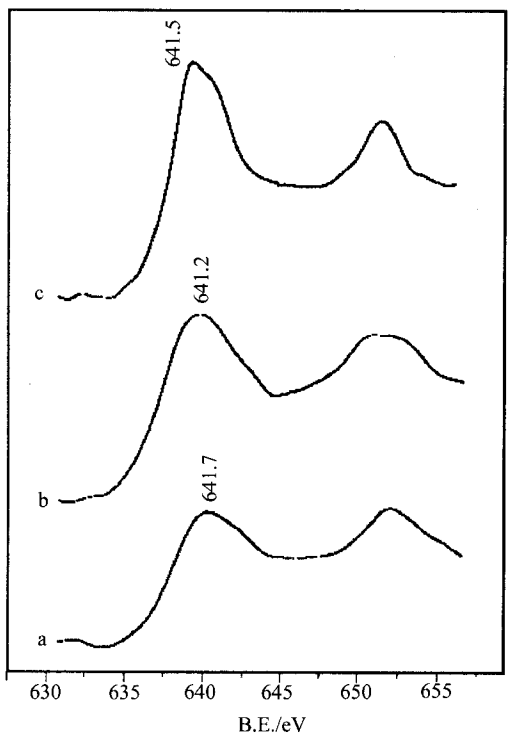

Fig. 7 XPS Mn(2p) spectra of 12Cu-10Mn/γ-Al_2O_3. (a) Before reduction; (b) After reduction; (c) After reaction.

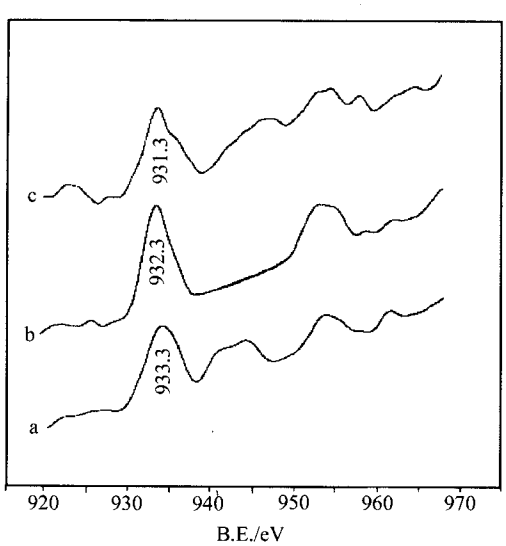

Fig. 8 XPS Cu(2p) spectra of 12Cu-10Mn/γ-Al_2O_3. (a) Before reduction; (b) After reduction; (c) After reaction.

be seen that the binding energy (B.E.) of the Cu(2p) level for the calcined catalyst was very close to that for pure CuO (B.E. = 933.3). In the reduced catalyst, the B.E. value of the Cu(2p) band was decreased to 932.3 eV, which contributed to the metallic copper. For the used catalyst, the XPS of Cu(2p) is 932.9, moreover, a shoulder peak (B.E. = 935) appears which is ascribed to the Cu^{2+}. The peak (B.E. = 932.9 eV) is contributed to Cu^{1+}. From the Fig. 8, it is concluded that the valence of Cu increases from zero in the reduced catalysts to +1 or +2 in the used catalysts. The XPS of Cu(2p) for the calcined, reduced and used 12Cu/γ-Al_2O_3 catalyst are shown in Fig. 9. From Fig. 9, it can be seen that the binding energy (B.E.) of the Cu(2p) level for the calcined catalyst was very close to that for pure CuO (B.E. = 933.3). In the reduced catalyst, the B.E. value of the Cu(2p) was decreased to 932.3 eV, which contributed to the metallic copper. For the used catalyst, the XPS of Cu(2p) is 932.4 which is very close to the B.E. of Cu^0. From Fig. 7, 8 and 9, it can be seen that Cu^+ existed on the working surface of the used Cu-Mn/γ-Al_2O_3 catalysts, while, Cu^0 existed on the Cu/γ-Al_2O_3 catalyst. It can be concluded that the catalytic activity was promoted by Cu with part of positive charge which was formed by means of long path exchange function between Cu—O—Mn.

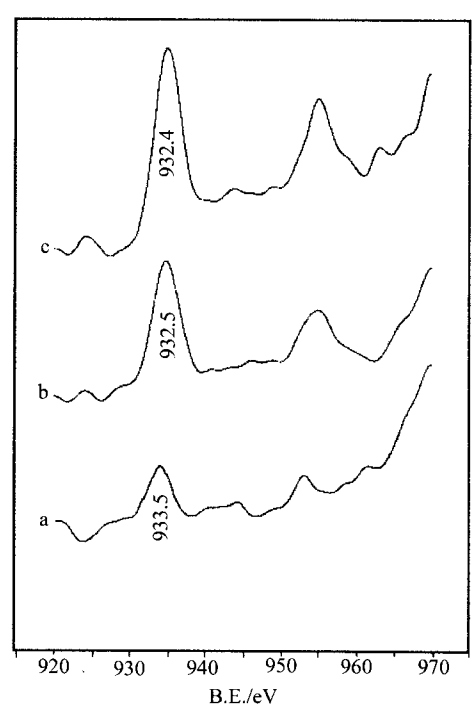

Fig. 9 XPS of Cu(2p) for 12Cu/γ-Al_2O_3 catalyst. (a) Before reduction; (b) After reduction; (c) After reaction.

Conclusion

In this paper, the effect of manganese on the dispersion, reduction behavior and active states of surface

of supported copper oxide catalysts have been investigated by XRD, temperature-programmed reduction and XPS techniques. The catalytic activity over CuO-MnO_x/γ-Al_2O_3 catalyst for CO_2 hydrogenation is higher than that of CuO/γ-Al_2O_3. The activity of methanol synthesis from CO_2/H_2 increases with the increasing the area of metallic copper. XRD result shows that the addition of manganese is beneficial in enhancing the dispersion of the supported copper oxide. The TPR results show that strong interaction between the copper and manganese oxide took place which causes the TPR peak of the CuO-MnO_x/γ-Al_2O_3 catalyst different from the individual supported copper and manganese oxide catalysts. For the CuO/γ-Al_2O_3 catalyst there are two reducible copper oxide species; α and β peaks are attributed to the reduction of highly dispersed copper oxide species and bulk CuO species respectively. For the CuO-MnO_x/γ-Al_2O_3 catalyst, four reduction peaks are observed. α peak is attributed to the dispersed copper oxide species; β peak is ascribed to the bulk CuO; γ peak is attributed to the reduction of high dispersed CuO interacting with manganese; δ peak may be the reduction of the manganese oxide interacting with copper oxide. XPS results show that Cu^+ mostly existed on the working surface of the Cu-Mn/γ-Al_2O_3 catalysts, while, for the Cu/γ-Al_2O_3 catalyst, Cu^0 mostly existed on the working surface. The activity was promoted by Cu with positive charge which was formed by means of long path exchange function between Cu—O—Mn. These results indicate that there is synergistic interaction between the copper and manganese oxide, which is responsible for the high activity of CO_2 hydrogenation.

References

1 Weatherbee, G. D.; Bartharomew, C. H. *J. Catal.* **1981**, *68*, 67.

2 Inui, T.; Funabiki, M.; Takegami, Y. *J. Chem. Soc.* **1980**, *1*, 76.

3 Solimosi, F.; Erdoheli, A. *J. Mol. Catal.* **1980**, *8*, 471.

4 Fujiwara, M.; Kiffer, R.; Hisanori A. *Appl. Catal.* **1997**, *154*, 87.

5 Frohlich, G.; Kestel, U.; Lojeweska, J. *Appl. Catal.* **1996**, *134*, 1.

6 Denise, B.; Sneeden, R. P. A. *J. Mol. Catal.* **1982**, *17*, 359.

7 Dubois, J. L.; Sayama, K.; Arakawa, A. *Chem. Lett.* **1982**, 1115.

8 Brown, J. A.; Homs, N.; Bell, A. T. *J. Catal.* **1990**, *124*, 73.

9 Waiwright, M.; Trimm, D. *Catal. Today* **1995**, *23*, 29.

10 Kitajima, N.; Hikichi, S.; Tanaka, M. *J. Am. Chem. Soc.* **1993**, *115*, 5496.

11 Klier, K. *Adv. Catal.* **1982**, *31*, 242.

12 Inui, T.; Takeguchi, T. *Catal. Today* **1991**, *10*, 95.

13 Bart, J. C. J.; Sneeden, R. P. A. *Catal. Today* **1987**, *2*, 1.

14 Chinchen, G. C.; Denny, P. J.; Jennings, J. R.; Spencer, M. S.; Waugh, K. C. *Appl. Catal.* **1988**, *36*, 1.

15 Sun, Q.; Zhang, Y.-L.; Chen, H.-Y.; Deng, J.-F.; Wu, D.; Chen, S.-Y. *J. Catal.* **1997**, *167*, 92.

16 Kotowski, W. *GB 2 025 418*, **1980** [*Chem. Abstr.* **1980**, *92*, 217862s].

17 Kotowski, W. *GB 2 025 252*, **1980** [*Chem. Abstr.* **1980**, *93*, 10657d].

18 Huang, H. K. *J. Mol. Catal.* **1991**, *64*, 53.

19 Li, J.-T.; Zhang. W.-D.; Gao, L.-Z. *Fenzi. Cuihua* **1997**, *11*, 369 (in Chinese).

20 Herman, R. G; Klier, K; Simmons, G; Finn, B. P; Bulko, J. W.; Kobylinski, T. P. *J. Catal.* **1979**, *56*, 407.

21 Mehta, S; Simmons, G. W; Klier, K; Herman, R. G. *J. Catal.* **1979**, *57*, 339.

22 Friedman, R. M; Freeman, J. J; Lytle, F. W. *J. Catal.* **1978**, *55*, 10.

23 Wollner, A; Lange, F. *Appl. Catal.* **1993**, *94*, 181.

(E200011260 LI, L. T.; LING, J.)